Reply to Community Comment:

Thank you for your valuable comments. We have addressed each of your concerns point-by-point as follows:

(1) *The authors use the Darcy-Brinkman-Stokes equations to simulate flow processes. However, further clarification on the rationale behind selecting this specific model over other commonly used approaches like MODFLOW-CFP would enhance understanding.*

We sincerely appreciate your valuable suggestions, which are crucial for improving the quality of our paper. In the revised manuscript, we have clarified the rationale for selecting the DBS model: the DBS model can simulate saturated-unsaturated flow by coupling free flow and seepage flow.

Lines 92-94:"Although MODFLOW-CFP is relatively comprehensive for regional karst groundwater simulation studies, the current version of MODFLOW-CFP only supports modeling single-phase groundwater flow."

Lines 106-108:"However, this approach lacks a built-in conduit flow solution scheme, making it difficult to adequately address the coupling requirements between rapid conduit flow and porous media seepage in karst areas."

(2) *Although the model captures complex interactions, the paper could benefit from a discussion of how simplifying assumptions (e.g., homogeneous permeability assumptions or simplified boundary conditions) affect the results' robustness and applicability.*

We sincerely appreciate your valuable suggestions, which are instrumental in enhancing the quality of our manuscript. In the revised version, we have added a comprehensive discussion on both the advantages and limitations of the DBS model:

Lines 343-351:

"2.4.1 DBS Model Conversion and Applicability Assessment

As illustrated in Figure 2, the Navier-Stokes (N-S) model can resolve fine-scale pore-scale flows and perform high-fidelity simulations. In contrast, the CFPv2 model achieves high computational efficiency and stability by discretizing one-dimensional conduits within porous media. The DBS (Dual-domain Brinkman-Stokes) model combines the advantages of both approaches: By incorporating additional resistance source terms into the N-S equations, it maintains high-fidelity flow resolution in conduits. For porous media, it adopts a Darcy-type flow formulation, significantly reducing computational costs."

Lines 1208-1213:

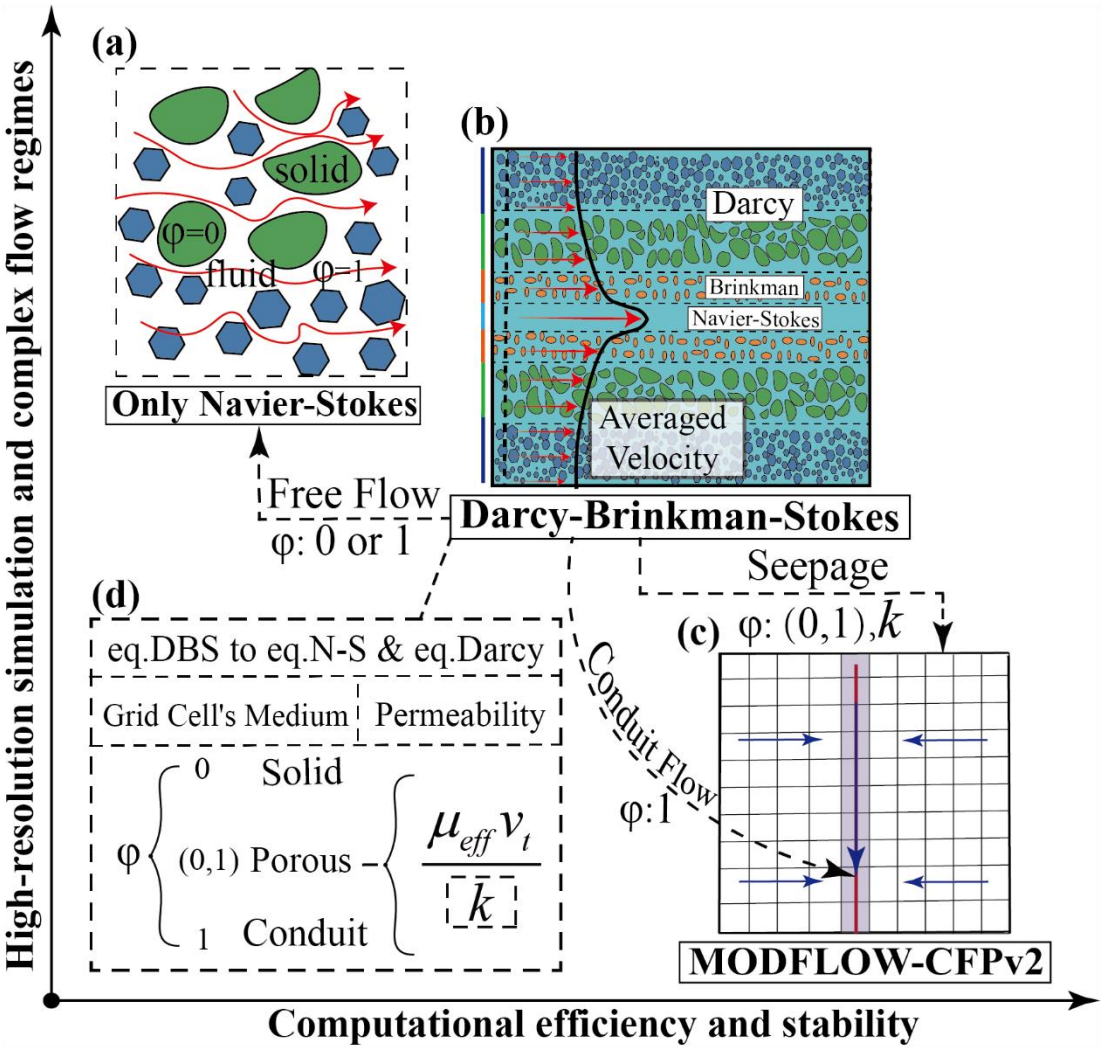

Figure 2. Diagram of performance and applicability of different models, (a) N-S model (Navier-Stokes model) , (b) DBS model, (c) Schematic diagram of MODFLOW-CFP model solution, (d) Conversion method from DBS equations to N-S equations and Darcy equations. “

(3) *Sensitivity and Uncertainty Analysis:*

The manuscript currently lacks a detailed sensitivity or uncertainty analysis, which is important to understand how variations in critical parameters (e.g., permeability, porosity, precipitation patterns) might affect the interaction processes described.

We sincerely appreciate your valuable suggestions, which are instrumental in enhancing the quality of our manuscript. The new “4. Uncertainty Analysis” section (lines 810-930) demonstrates that:

(1) Conduit geometry (square cross-sections yield higher peak flows than circular ones)

(2) Permeability of the epikarst zone (higher permeability increases inter-media exchange frequency)
are key factors regulating karst-stream exchanges. This provides prioritization guidance for model parameter calibration.
Lines 810-930:

"4. Uncertainty Analysis and Discussion

The multi-level conduit configuration inherently affects multi-media interactions by simultaneously altering permeability, conduit diameter, and porosity parameters. This study will further conduct sensitivity analyses on individual variables to investigate their impacts on the vulnerability of karst aquifer systems.

4.1 Impacts of Conduit Diameter and Geometry on Interactions Between Karst Aquifer Systems and Streams

Fig. 12 presents hydrographs under conditions of circular conduits with varying radii (r=0.2, 0.3, 0.3, and 0.5 m) and square-section conduits (r=0.5 m) for (a) stream-connected flow, (b) karst spring discharge, (c) epikarst flow, (d) porous medium I (PM I), (e) PM II, and (f) PM III. Fig. 12(c.1) illustrates different conduit cross-sectional shapes to analyze their impacts on the interactive flow between karst aquifer systems and adjacent streams.

As shown in Fig. 12(a), larger conduit radii correspond to higher initial discharge peaks and shorter peak arrival times, indicating enhanced porous medium recharge and faster fluid transmission through larger conduits. Notably, the square-section conduit (s-r_c=0.5) exhibits higher peak discharge than its circular counterpart (rc=0.5) due to its surplus cross-sectional area accommodating greater fluid discharge under identical nominal radii.

Fig. 12(b) demonstrates that karst spring peak discharge increases with conduit radius. At r=0.5 m, the square-section conduit (s-r_c=0.5) achieves higher peak discharge than the circular conduit (r_c=0.5), but displays lower recession flow. This occurs because identical precipitation infiltration recharge leads to greater porous medium storage depletion during peak periods in square conduits, subsequently reducing porous medium-to-conduit recharge during baseflow recession.

Combined analysis of Figs. 12(c), (d), and (e) reveals that conduit radius variations do not significantly affect epikarst hydrographs or PM I/II hydrographs. However, square-section sinkholes modify flow patterns: epikarst hydrographs show lower values under square conduits, while PM I/II hydrographs exhibit higher values due to enhanced epikarst groundwater collection in square cross-sections, increasing recharge to PM I/II.

Fig. 12(e) indicates that larger conduit radii correspond to lower negative values. Combined with Fig. 12(a), this demonstrates that increased stream recharge through larger conduits elevates both stream peak discharge and water levels, thereby enhancing porous medium-stream

interactions. Similarly, Fig. 12(f) shows that larger conduit radii increase karst spring discharge and PM III hydrograph elevation through enhanced gravity-driven groundwater recharge.

Conduit geometry (radius and shape) constitutes a critical factor in karst aquifer hydrological modeling. Larger circular conduits accelerate peak discharge arrival and amplify stream-connected flow peaks and karst spring discharge. Square-section conduits outperform circular equivalents in peak discharge capacity under identical nominal radii due to cross-sectional area advantages. Enlarged conduits intensify porous medium-stream interactions and amplify PM III recharge through gravitational effects. Comprehensive consideration of conduit geometry impacts on hydrological elements is essential for improving model accuracy and reliability in simulating karst aquifer-stream interaction processes.

4.2 Influence of Permeability on the Interaction Processes Between Karst Aquifer Systems and Streams

The permeability of the epikarst directly controls the ease of fluid infiltration from the surface into the conduit system. Fig. 13 illustrates the hydrological process curves under different epikarst permeability coefficients (K_E=10^{-6}, 10^{-7}, 10^{-8}, 10^{-9}; when K_E=10^{-9}, the permeability matches that of porous media, rendering the epikarst incapable of rapid groundwater leakage) for: (a) stream, (b) karst spring, (c) epikarst, (d) PM I, (e) PM II, and (f) PM III. This aims to reveal how epikarst permeability regulates groundwater flow patterns in complex conduit systems and intermedia interactions.

As shown in Fig. 13(a), under high epikarst permeability (K_E=10^{-6}): the discharge curve rises rapidly to a peak of ~4.5 m^3/s followed by a sharp decline. This indicates that high permeability enables rapid groundwater leakage from the epikarst to the stream, causing swift flow increases. Peak stream discharge diminishes with decreasing permeability. High permeability reduces flow resistance, facilitating faster fluid entry into the conduit system and generating sharp discharge peaks, while low permeability increases resistance, resulting in gradual fluid release and broader, lower discharge curves.

Fig. 13(b) demonstrates that epikarst permeability differences from porous media have minimal impact on conduit flow. However, when epikarst permeability equals that of porous media (K_E=10^{-9}), the peak discharge at the karst spring decreases while maintaining identical baseflow recession characteristics. Combining Figs. 13(c) and (c.1), higher epikarst permeability enhances lateral discharge to the stream. At K_E=10^{-9}, gravitational forces dominate vertical recharge to lower media without lateral discharge.

Fig. 13(d) reveals decreasing discharge from Porous Medium I to the stream with reduced epikarst permeability. Cross-referencing Figs. 13(a) and (e), lower epikarst permeability reduces both stream discharge and water level, limiting recharge to Porous Medium II. Fig. 13(f) shows negligible epikarst permeability influence on Porous Medium III's hydrograph.

Epikarst permeability constitutes a critical factor in hydrological modeling of karst aquifer systems. Highly permeable epikarst produces rapid streamflow peaks followed by sharp declines,

reflecting efficient groundwater leakage to the stream. Conversely, low permeability yields diminished peaks and broader discharge curves. While karst spring discharge remains relatively stable when epikarst permeability differs from porous media, proper characterization of epikarst permeability is essential for accurately simulating hydraulic interactions between media, regulating groundwater flow pathways and velocities. This enhances model reliability in capturing complex flow dynamics within karst conduit-stream systems.

4.3 Influence of Porosity on the Interaction Between Karst Aquifer Systems and Adjacent Streams

Fig. 14 presents the hydrographic process curves under different porosity conditions (φ=0.4, φ =0.3, φ =0.2, φ =0.1) for (a) stream, (b) karst spring, (c) epikarst, (d) PM I, (e) PM II, and (f) PM III. Fig. 14(c.1) illustrates the schematic diagram of groundwater flow under different pore sizes. The study aims to elucidate how porosity regulates fluid flow patterns in complex conduit systems.

As shown in Fig. 14(a), lower porosity results in higher flow peaks and earlier peak times. This occurs because reduced pore space limits groundwater storage capacity, forcing excess water to discharge rapidly and elevating the stream hydrograph. Fig. 14(b) demonstrates that lower porosity drives groundwater to preferentially flow through karst conduits and discharge at springs. In Fig. 14(c), the peak discharge of epikarst at φ =0.4 slightly exceeds those at φ =0.3, φ =0.2, and φ =0.1.

Fig. 14(d) reveals that at φ =0.1, the storage capacity of porous medium I reaches critical limits. Groundwater recharged from epikarst to porous medium I is rapidly discharged, resulting in significantly higher discharge rates compared to φ =0.3, φ =0.2, and φ =0.1. Fig. 14(e) indicates increased discharge from porous media to the stream as porosity decreases. Combined with Fig. 14(a), reduced porosity enhances stream stage and discharge but diminishes the stream's ability to recharge porous media due to limited storage capacity. Fig. 14(f) shows negligible porosity effects on the hydrograph of porous medium III, as its behavior is primarily governed by conduit flow.

In hydrological modeling, porosity parameters must be calibrated to accurately simulate groundwater flow paths and storage-release dynamics. For low-porosity regions, models should emphasize rapid drainage capacity of conduit systems and transient flow variations. In high-porosity areas, considerations should include fluid retention risks, stream-porous media interactions, and their long-term impacts on geological stability and water resource allocation. Proper porosity parameterization enhances simulation accuracy for diverse hydrological processes, enabling improved prediction and management of karst water resources.

Karst hydrological vulnerability manifests prominently through rapid infiltration, epikarst runoff, groundwater table fluctuations, and abrupt spring discharge variations. The DBS model effectively simulates multi-media interactions during extreme recharge events, enabling temporal

analysis of media-stream exchanges, identification of peak interaction values, and applications in coupled conduit flow-seepage processes for two-phase flow systems."

Lines 1257-1275:

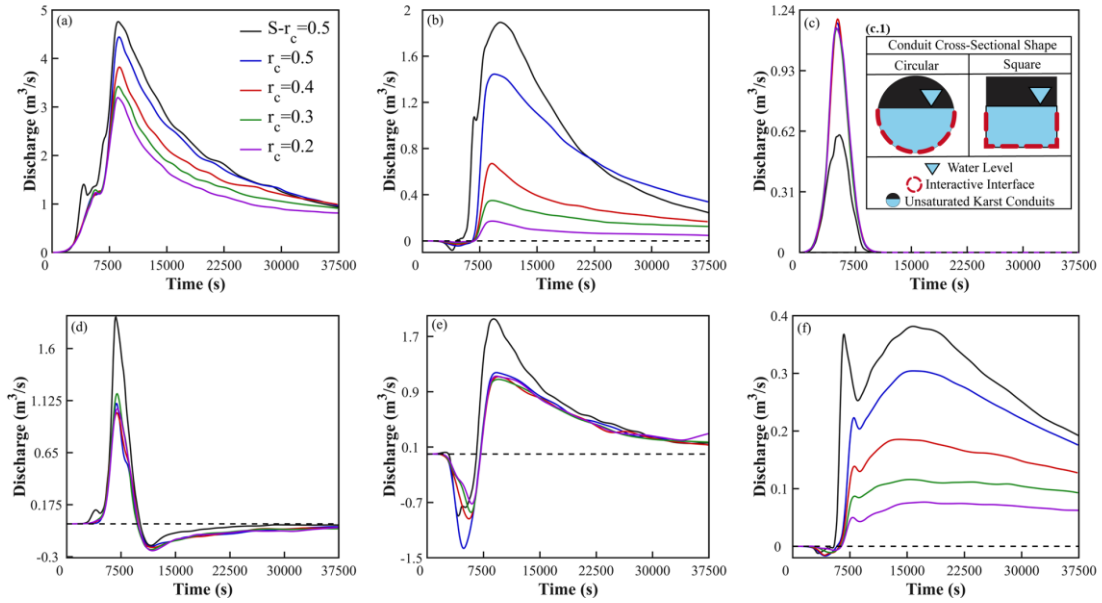

Figure 12. Hydrological process curves for (a) stream, (b) karst spring, (c) epikarst, (d) PM I, (e) PM II, and (f) PM III under conditions of circular conduits with radii r_c = 0.2, 0.3, 0.3, and 0.5, and square-cross-section conduits with S-r_c = 0.5. Subplot (c.1) shows a schematic diagram of different conduit cross-sectional shapes.

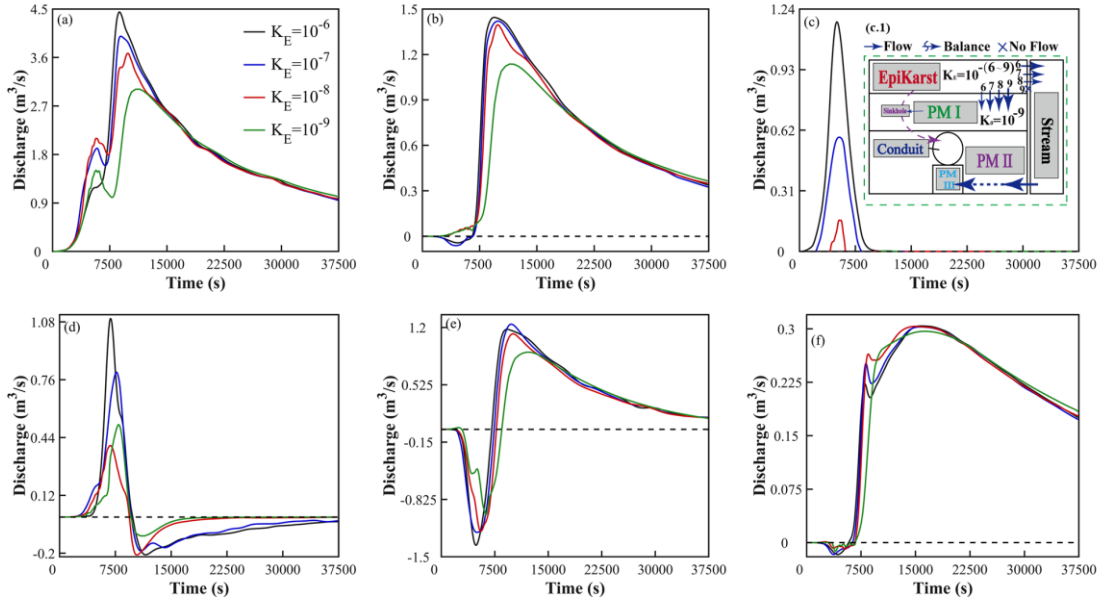

Figure 13. Hydrographs under different epikarst permeability conditions (K_E=10^{-6}, K_E=10^{-7}, K_E=10^{-8}, K_E=10^{-9}) for: (a) stream, (b) karst spring, (c) epikarst, (d) PM I, (e) PM II, (f) PM III. Subfigure (c.1) shows a schematic diagram of media interactions under varying epikarst

permeability conditions.

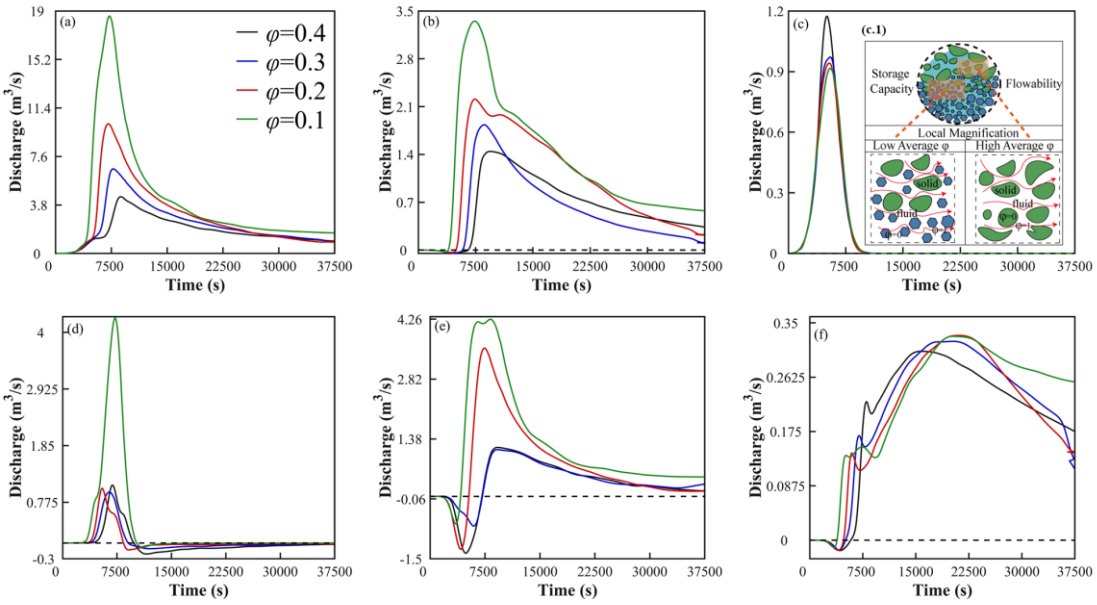

Figure 14. hydrograph curves under different porosity conditions (φ = 0.4, φ = 0.3, φ = 0.2, φ = 0.1) for (a) stream, (b) karst spring, (c) epikarst, (d) PM I, (e) PM II, and (f) PM III. Among these, (c.1) illustrates a schematic diagram of the medium's water storage capacity and flow capacity under varying porosity conditions."

(4) *The modeling approach is theoretical and numerical. Adding validation using real-world or field observation data could greatly strengthen confidence in the model's predictive capability and practical applicability.*

We sincerely appreciate your valuable suggestions, which are crucial for enhancing the quality of our manuscript.

Given the technical challenges in in-situ monitoring of multi-media exchange fluxes, we validated the DBS model's capabilities in variably saturated flow modeling using classical experimental cases (Warrick et al., 1985; Vauclin et al., 1979) (lines 712-735). We are currently collaborating with karst field sites to obtain observational field data.

Lines 712-735:

" The external recharge of the system significantly influences the interaction processes among different media. This study further investigates how the inherent hydrogeological properties of karst systems affect these interactive processes. Variable saturated flow in the karst vadose zone plays a critical role (Dvory et al., 2018), where the water retention characteristics of porous media govern unsaturated flow dynamics. However, the CFPv2 model struggles to simulate variable saturation processes. This paper compares the DBS model results with two distinct experimental datasets to elucidate the advantages and limitations of the DBS approach in simulating variable saturated flow.

Case 1: A typical unsaturated-unsteady seepage problem in sandy clay loam (Warrick et al., 1985), where the soil hydraulic properties are provided by the international UNSODA database (Leij et al., 1996). Key parameters include: k = 1 × 10−6 m/s, α_s = 0.363, α_r = 0.186, and n = 1.53. The model consists of a vertical soil column (1 m thickness) with an initial pressure head of -8 m across the domain. The top boundary is set to a pressure head of 0 m to simulate free surface infiltration.

Case 2: A 2D laboratory infiltration experiment by Vauclin et al. (1979), widely used for evaluating saturated-unsaturated unsteady seepage models. The soil slab measures 2.00 m in height, 6.00 m in width, and 0.05 m in thickness, with an impermeable base and free drainage boundaries on both sides. Initially, the water table is set at 0.65 m. A central 1.00 m section of the top boundary receives uniform precipitation at 0.148 m/h for 8 hours, during which free surface evolution is monitored. Soil hydraulic properties are described using the van Genuchten-Mualem model with parameters: k = 0.35 m/h, α_s = 0.30, α_r = 0.01. Due to symmetry, the DBS model simulates the right half of the domain."

(5) *The authors mention fine grid discretization and the Courant number limitations causing small time steps, which implies significant computational costs. A brief discussion of the computational resources required and possible strategies for optimization could enhance the practicality and usability of their approach.*

We sincerely appreciate your valuable suggestions, which are crucial for enhancing the quality of our manuscript. The DBS model computations in this study were performed on a Lenovo ThinkSystem SR665 computational server, with optimization strategies relying on domain decomposition-based parallelization.

Lines 352-357:

"However, the DBS model operates in three dimensions (3D), requiring grid refinement around conduits and their vicinity to ensure accurate flow resolution. This increases computational load compared to the 1D conduit flow framework of CFPv2. To address this challenge, all simulations in this study were executed on a Lenovo ThinkSystem SR665 server, which provides the necessary computational power for handling complex 3D meshes."

(6) *While the comparison with MODFLOW-CFP is insightful, the manuscript could benefit from clearly highlighting specific scenarios or conditions under which the presented model notably outperforms or underperforms compared to MODFLOW-CFP.*

We sincerely appreciate your valuable suggestions, which are crucial for enhancing the quality of our manuscript. We conducted a comparative analysis of the DBS model and CFPv2 model performance.

Lines 343-351:

“2.4.1 DBS Model Conversion and Applicability Assessment

As illustrated in Figure 2, the Navier-Stokes (N-S) model can resolve fine-scale pore-scale flows and perform high-fidelity simulations. In contrast, the CFPv2 model achieves high computational efficiency and stability by discretizing one-dimensional conduits within porous media. The DBS (Dual-domain Brinkman-Stokes) model combines the advantages of both approaches: By incorporating additional resistance source terms into the N-S equations, it maintains high-fidelity flow resolution in conduits. For porous media, it adopts a Darcy-type flow formulation, significantly reducing computational costs.”

Lines 1208-1213:

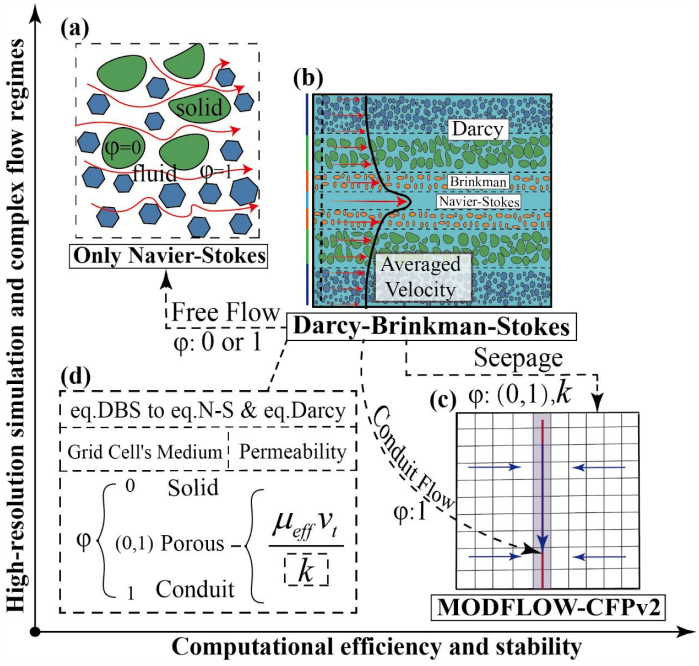

Figure 2. Diagram of performance and applicability of different models, (a) N-S model (Navier-Stokes model) , (b) DBS model, (c) Schematic diagram of MODFLOW-CFP model solution, (d) Conversion method from DBS equations to N-S equations and Darcy equations. “

(7) I highly recomment to expand your literature review to the integrated models such as SWAT-MODLOW, which are important aspect of your work, I recommend you to cite below papers.Hydrogeological modelling of a coastal karst aquifer using an integrated SWAT-MODFLOW approach ---- Estimating exploitable groundwater for agricultural use under environmental flow constraints using an integrated SWAT-MODFLOW model --- Can Large Language Models Effectively Reason about Adverse Weather Conditions?

We sincerely appreciate your valuable suggestions, which are crucial for enhancing the quality of our manuscript. In the Introduction (Lines 85-90), we have added a discussion on integrated modeling approaches (e.g., SWAT-MODFLOW), citing your recommended references (Fiorese et al., 2025; Yifru et al., 2024).

Lines 85-90:

“ Moreover, this methodology has been extensively applied worldwide for estimating karst groundwater flow and water resources (Chang et al., 2015; Qiu et al., 2019; Kavousi et al., 2020; Gao et al., 2020, 2024), as well as in integrated modeling studies coupling SWAT with MODFLOW to investigate groundwater-surface water interactions (Fiorese et al., 2025; Yifru et al., 2024).”